

# Decrease in magnetosheath jet production due to conditions within Coronal Mass Ejections

Florian Koller<sup>1</sup>, Ferdinand Plaschke<sup>2</sup>, Manuela Temmer<sup>3</sup>, Luis Preisser<sup>4</sup>, Owen Roberts<sup>4</sup>, Stefan Weiss<sup>1</sup>, and Zoltán Voros<sup>5</sup>

<sup>1</sup>Institute for Geophysics, Astrophysics and Meteorology, University of Graz

<sup>2</sup>Institut für Geophysik und extraterrestrische Physik

<sup>3</sup>Institute for Geophysics, Astrophysics and Meteorology, University of Graz, Universitätsplatz 5, A-8010 Graz, Austria

<sup>4</sup>Space Research Institute

<sup>5</sup>Space Research Institute, Austrian Academy of Sciences

November 24, 2022

## Abstract

Magnetosheath jets are dynamic pressure enhancements observed in the terrestrial magnetosheath. Their generation mechanisms are currently debated but can be linked to foreshock processes. Recent results showed that jets are less numerous when coronal mass ejections (CME) cross the magnetosheath. Here, we show for the first time how CMEs and their magnetic ejecta (ME) region are related to jet production. Based on THEMIS and OMNI data covering 2008–2021, we show the probability distribution of jet production in 2D parameter histograms using the IMF cone angle and Alfvén Mach number. We compare this distribution with the values within CME-MEs. We find high cone angles and low Alfvén Mach numbers within CME-MEs, which both are unfavorable for jet production as they may inhibit a proper foreshock region. We predict that future missions, measuring the magnetosheath of Mercury, will find low numbers of jets due to low Alfvén Mach numbers.

# Decrease in magnetosheath jet production due to conditions within Coronal Mass Ejections

Florian Koller<sup>1</sup>, Ferdinand Plaschke<sup>2</sup>, Manuela Temmer<sup>1</sup>, Luis Preisser<sup>3</sup>, O. W. Roberts<sup>3</sup>, Stefan Weiss<sup>1</sup>, Zoltan Vörös<sup>3,4</sup>

<sup>1</sup>Institute of Physics, University of Graz, Universitätsplatz 5, 8010 Graz, Austria

<sup>2</sup>Institut für Geophysik und extraterrestrische Physik, TU Braunschweig, Mendelssohnstraße 3, 38106

Braunschweig, Germany

<sup>3</sup>Space Research Institute, Austrian Academy of Sciences, Schmiedlstrasse 6, 8042 Graz, Austria

<sup>4</sup>Institute of Earth Physics and Space Science, ELRN, Csatkai E. u. 6-8, 9400 Sopron, Hungary

## Key Points:

- The low number of jets observed during CMEs come from high cone angles and low Alfvén Mach numbers related to the magnetic ejecta.
- We show how both parameters are distributed during times of jet observation compared to reference solar wind times.
- The condition found in CMEs regarding cone angle and Mach number are unfavorable for jet production, hence CMEs decrease the jet occurrence.

---

Corresponding author: Florian Koller, [florian.koller@uni-graz.at](mailto:florian.koller@uni-graz.at)

**Abstract**

Magnetosheath jets are dynamic pressure enhancements observed in the terrestrial magnetosheath. Their generation mechanisms are currently debated but can be linked to foreshock processes. Recent results showed that jets are less numerous when coronal mass ejections (CME) cross the magnetosheath. Here, we show for the first time how CMEs and their magnetic ejecta (ME) region are related to jet production. Based on THEMIS and OMNI data covering 2008–2021, we show the probability distribution of jet production in 2D parameter histograms using the IMF cone angle and Alfvén Mach number. We compare this distribution with the values within CME-MEs. We find high cone angles and low Alfvén Mach numbers within CME-MEs, which both are unfavorable for jet production as they may inhibit a proper foreshock region. We predict that future missions, measuring the magnetosheath of Mercury, will find low numbers of jets due to low Alfvén Mach numbers.

**Plain Language Summary**

The Sun produces a constant outflow of particles and magnetic field, the solar wind. The Earth’s magnetic field diverts that flow and protects us from these particles. A shock wave is built up between the magnetic field and the solar wind. Here, the particles get decelerated abruptly and form a turbulent region: the Earth’s magnetosheath. Within the magnetosheath, we regularly find faster or denser flows of particles, which we call jets. How these jets get formed is part of active research. We look at times where the Sun bursts out huge particle clouds (coronal mass ejections, CMEs) in the direction of Earth and analyze, how these clouds affect the jet generation. We compare, how the conditions in the solar wind differ from the conditions in CMEs. Specifically, we look at values that affect the shock: the angle of the magnetic field and the Mach number. We then compare, how the conditions in the solar wind looks when jets get generated. We find that the CME decreases the generation of jets with its strong magnetic field and its rather randomly distributed magnetic field angle. With that, the CME change the properties of the bow shock and therefore the jet generation mechanisms.

**1 Introduction**

The magnetosheath is the region of shocked solar wind (SW) plasma sunward of the Earth’s magnetosphere. First noticed by Němeček et al. (1998), the magnetosheath regularly shows dynamic pressure enhancements, which we shall call jets in the present work. Jets can show an increase in dynamic pressure up to 15 times compared to the surrounding plasma (Plaschke et al., 2013). Their median size is estimated to be  $0.1 R_e$  but can reach up to more than  $2 R_e$  (Plaschke et al., 2016, 2020). Large jets in particular can be geoeffective (Hietala et al., 2018; Nykyri et al., 2019; Norenus et al., 2021) and appear several times per hour (Plaschke et al., 2016).

Recently, several generation mechanisms were proposed to explain the occurrence of magnetosheath jets. We briefly describe those discussed in the literature, reviewed in Plaschke et al. (2018). Most mechanisms explain jets as a result of different processes in the foreshock region and are therefore associated with the quasi-parallel bow shock. The foreshock can only build up due to back-streaming ions from a super-critical bow shock and is therefore dependent on a high Alfvénic Mach number (Balogh & Treumann, 2013), which is defined as  $M_A = v_{sw}/v_A$ , with  $v_{sw}$  denoting the SW velocity, and  $v_A = B/\sqrt{\mu_0\rho}$  (with B being the magnetic field strength,  $\mu_0$  the magnetic permeability and  $\rho$  the SW density, respectively) defining the Alfvén velocity. The foreshock builds up sunward of the quasi-parallel shock front and therefore requires a low shock normal angle  $\Theta_{Bn}$ . The interplanetary magnetic field (IMF) cone angle ( $\arccos|B_x|/|B|$ , with  $B_x$  denoting the magnetic field strength in GSE-X) is often used as a substitute for  $\Theta_{Bn}$  for

66 the subsolar region (see e.g. Plaschke et al., 2013; Vuorinen et al., 2019; Raptis et al.,  
67 2020).

68 In general, results show that jets appear more often during low cone angle periods  
69 (Plaschke et al., 2013; Vuorinen et al., 2019; LaMoury et al., 2021). Phenomena in the  
70 foreshock can cause ripples in the bow shock (Balogh & Treumann, 2013). The way in  
71 which the SW is processed by the rippled shock has been proposed to be the cause for  
72 jet generation (Hietala et al., 2009; Hietala & Plaschke, 2013; Preisser et al., 2020). At  
73 the ripple, the local oblique shock front may cause the deceleration of the incoming SW  
74 plasma to be less efficient in the GSE-X direction in comparison to the less oblique shock  
75 surroundings. It would create a flow (jet) in the downstream side of the shock that is  
76 faster than the surrounding shocked and decelerated plasma. This rippling effect as well  
77 as the integration of fast foreshock flows into the magnetosheath might also be a con-  
78 sequence of short large-amplitude magnetic field structures (SLAMS) forming in the fore-  
79 shock (Schwartz & Burgess, 1991; Karlsson et al., 2015). The latest simulations have shown  
80 that the majority of jets can be related to foreshock compressional structures (Suni et  
81 al., 2021). Recently, Raptis et al. (2022) presented evidence that jets can be generated  
82 as a consequence of the bow shock reformation process at the quasi-parallel shock front  
83 itself. This has been also proposed to be a mechanism for the formation of paramagnetic  
84 embedded plasmoids based on hybrid simulations (Preisser et al., 2020). Hietala and Plaschke  
85 (2013) estimated that the majority of jets can be associated to bow shock rippling. A  
86 subset of jets can be explained by other mechanisms. For example, Archer et al. (2012)  
87 suggested that rotational discontinuities in the magnetic field cause pressure pulses in  
88 the magnetosheath every time we see a change from the quasi-parallel to the quasi-perpendicular  
89 shock region and vice-versa.

90 In a recent statistical study Koller et al. (2022) analyzed jet occurrence within large  
91 scale SW structures, such as transient coronal mass ejections (CMEs) and stream inter-  
92 action regions (SIRs) together with their high speed streams (HSSs). It was found that  
93 jets are less frequent when the magnetic ejecta (ME) region of the CME passes Earth.  
94 In comparison to quiet SW conditions and compressed SW for SIRs, CMEs and their  
95 ME regions present “laboratories” with very different SW conditions. Typically, CMEs  
96 are faster than the SW and can drive shocks which generate two separate density struc-  
97 tures: compressed and piled up SW in the sheath and leading edge (see Temmer & Both-  
98 mer, 2022), followed by a strong and smoothly rotating magnetic flux rope. Fig. 1 shows  
99 a CME example measured by the Active Composition Explorer (ACE, Stone et al., 1998).  
100 In the present work, we therefore investigate on the basis of these recent results the phys-  
101 ical mechanism of the decrease in jet occurrence and suppression of jets. The results will  
102 give us a better understanding of jet production mechanisms. We hypothesize that the  
103 conditions inside the CME-ME pose difficulties for the building of a proper foreshock.  
104 Due to the twisted magnetic field lines in the flux rope inside of the ME, the IMF cone  
105 angle could differ greatly from radial IMF conditions. Radial IMF lines however seem  
106 to be a necessary condition to generate a quasi-parallel shock region that builds the fore-  
107 shock. In addition to that, the high magnetic field strength and low density inside a CME-  
108 ME cause an increase in Alfvén velocity. Thus, the Alfvén Mach number decreases, caus-  
109 ing a decrease in the strength of the bow shock. The sum of all these effects generated  
110 by the arrival of the CME-ME to the bow shock could inhibit the building of a foreshock  
111 region that can efficiently generate jets near the subsolar point.

112 To test our hypothesis, we look at jets detected by THEMIS spacecraft between  
113 2008 and 2021 and compare the SW conditions during these times.

## 114 2 Data

115 We compare in situ SW plasma and magnetic field data from OMNI during times  
116 when jets are observed with the SW measured during CMEs and as a reference during

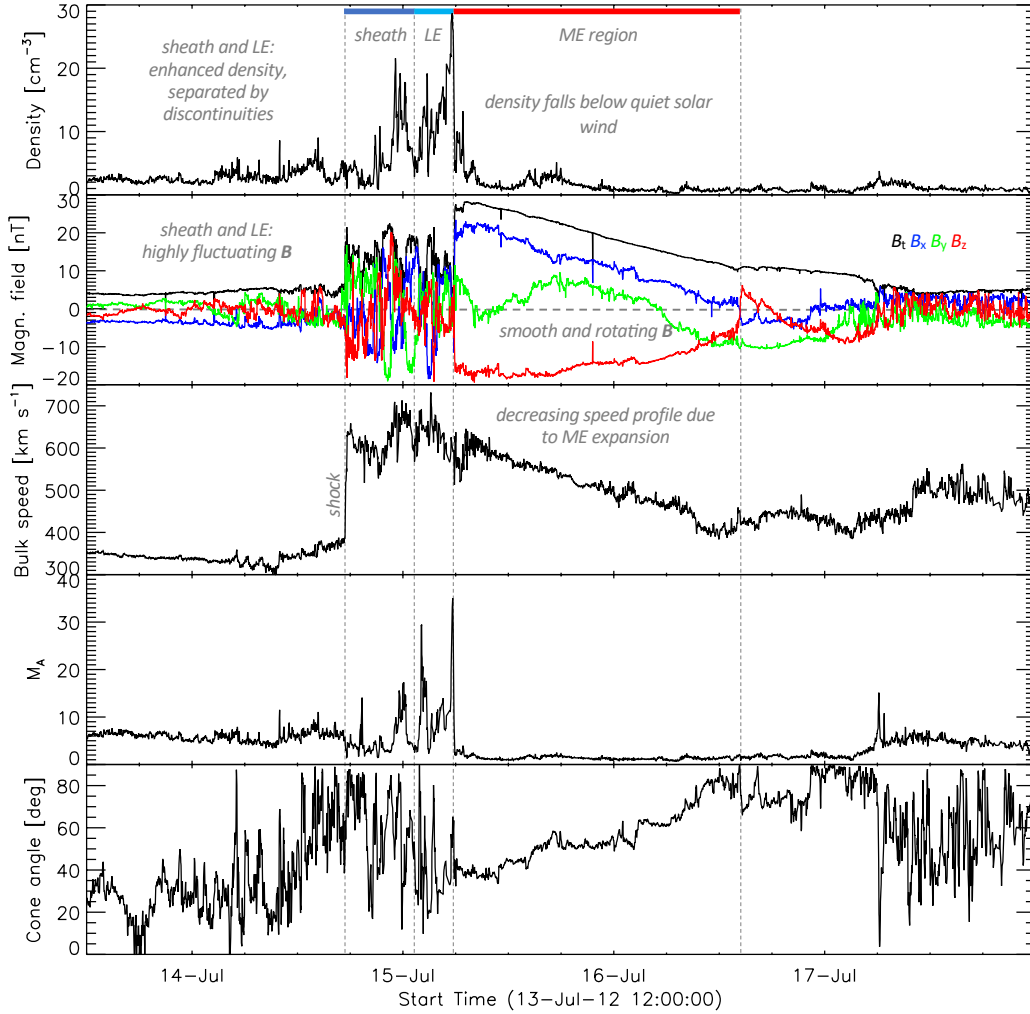


**Figure 1.** Example of a CME from ACE measurements. The three panels from top to bottom show the measured proton density, total magnetic field and vector components in GSE coordinates (see legend), and the proton bulk speed. This CME clearly reveals the typical structures, shock, two density enhancements — sheath (dark blue) and leading edge (LE, light blue) — followed by the ME with the twisted field components. The next two panels give the calculated Alfvénic Mach number and the cone angle (see more details in the text).

117 all times when magnetosheath data were available. We use 1-min resolution OMNI ve-  
 118 locity, magnetic field, and density data (King & Papitashvili, 2005). Our data covers the  
 119 time range between January 2008 and December 2021.

120 Data from the THEMIS spacecraft (Angelopoulos, 2008) are used to detect inter-  
 121 vals of jets in the magnetosheath. Specifically, we use the reduced ion moments from the  
 122 (ion velocity, density, temperature, and energy flux) from the THEMIS Electrostatic An-  
 123alyzer (ESA McFadden et al., 2008). We use magnetic field measurements from the Flux-  
 124gate Magnetometer (FGM Auster et al., 2008).

125 Magnetosheath intervals are determined by the same criteria used in Plaschke et  
 126 al. (2013) and Koller et al. (2022): The spacecraft GSE position is restricted to 7–18  $R_e$   
 127 and has to be within a 30° Sun-centered cone with tip at the Earth. To ensure that the  
 128 spacecraft is within the magnetosheath, the ion density has to be at least twice as dense  
 129 as the upstream solar wind. The energy flux of the 10 keV ions has to be less than those  
 130 of the 1 keV ions. The magnetosheath intervals are required to be longer than 2 min.

131 Jets were defined using the criteria of Archer and Horbury (2013):  $p_{\text{dyn}} > 2 \times$   
 132  $\langle p_{\text{dyn}} \rangle_{20\text{min}}$ . Here,  $\langle p_{\text{dyn}} \rangle_{20\text{min}}$  denotes the 20 minute running average of the magnetosheath  
 133 dynamic pressure. Therefore, enhancements of the dynamic pressure larger than two times  
 134 of the surrounding plasma within 20 minutes are declared as jets. Magnetosheath inter-  
 135 vals shorter than 20 minutes are not considered for jet detection. Jets were restricted  
 136 to only those with a duration of more than 5 seconds. Using these criteria, we detected  
 137 a total 51737 jets within the given time range. The intervals of magnetosheath and jet  
 138 times are provided at <https://osf.io/hwkum/> as given in Koller et al. (2022).

139 Arrival times of ICMEs at Earth are collected in an online catalogue maintained  
 140 by Richardson and Cane (Cane & Richardson, 2003; Richardson & Cane, 2010). It in-  
 141 cludes a variety of information on near-Earth CMEs that have been detected since 1996.  
 142 We use the start and end times of CME-MEs (labeled as ICME Plasma/Field Start, End)  
 143 in our work, which are the times that were measured by ACE.

### 144 3 Analysis

145 We calculate mean OMNI values during jet intervals and during all times when we  
 146 have simultaneously magnetosheath observations by THEMIS. The latter is used as a  
 147 reference to determine, how the SW parameters are distributed during jet detection times.  
 148 For each time interval, we calculate the mean SW Alfvénic Mach number and the IMF  
 149 cone angle. One mean Mach number and cone angle value was determined for each jet.  
 150 The SW reference conditions datapoints have a 1-min resolution. To check how impor-  
 151 tant these parameter are for the jet production, we plot a 2-dimensional (2D) histogram  
 152 with the cone angle on the x-axis and the Mach number on the y-axis. All histograms  
 153 are normalized to the peak value. Bin sizes of 4.8 ° for the x-axis and 1.6 for the y-axis  
 154 were chosen. These bin sizes ensure reliable amounts of data as well as reasonable res-  
 155 olution for our analysis.

156 We then determine the jet probability distribution as a function of Alfvén Mach  
 157 number and IMF cone angle. We do this by dividing the SW conditions that we find dur-  
 158 ing jets by the overall SW conditions. This results in a 2D histogram plot, where the jet  
 159 probability is color-coded in each bin. As a final analysis we check, how this jet prob-  
 160 ability distribution compares to the SW conditions that we find within CME-MEs.

### 161 4 Results

162 The left plot of Fig.2 shows the 2D histogram distribution for the SW condition  
 163 during all times when we have magnetosheath observations. The SW condition peak at  
 164 cone angles of 40–90 ° and Mach numbers around 6–12. This distribution serves as a ref-

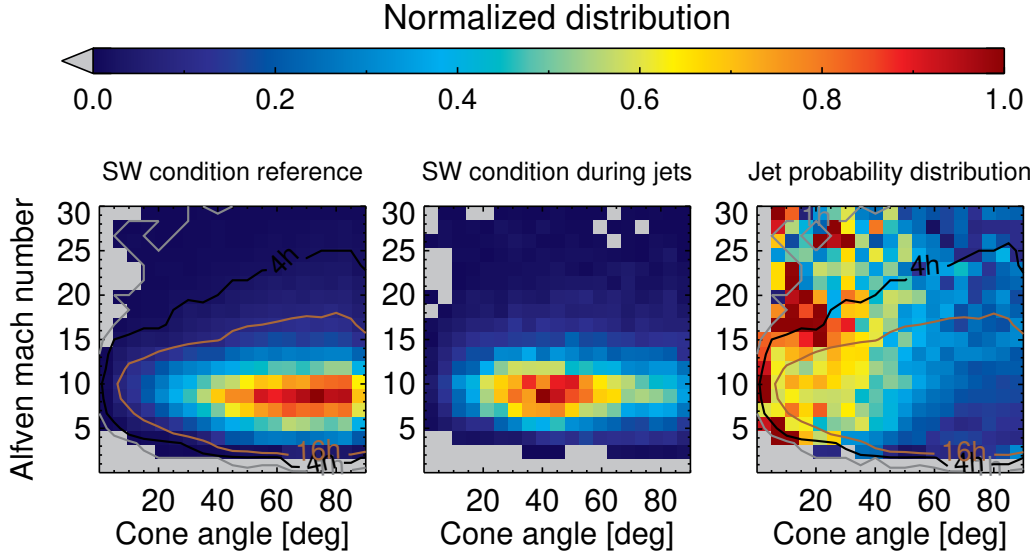


**Figure 2.** 2D histogram showing normalized distributions of cone angle and Mach number. The left plot shows the overall distribution of both parameter in the SW during all observation times. The middle plot shows the SW parameter distribution during jet detection. The right plot shows the jet probability depending of both parameters. Contours indicate, how many hours of data we have for each bin. Most reliable data are marked by the 16 h contour (in brown).

165 erence for the further analysis. The distribution of SW conditions during jets is shown  
 166 in the middle plot of Fig. 2. We find that jets appear dominantly during cone angles of  
 167 20–50 and Mach numbers of 6–11.

168 The right plot of Fig. 2 shows the normalized jet probability. Here, the distribu-  
 169 tion of SW condition during jets is divided by the reference SW distribution. Contours  
 170 on this figure show the amount of available magnetosheath observation time per bin. It  
 171 represents the data from the reference values. The innermost contour (in brown) indi-  
 172 cates that within this area, each bin in the 2D plot consists of 16 h or more of magne-  
 173 tosheath observation time, making these areas the most reliable to our analysis. As ex-  
 174 pected, the jets are found predominantly at lower cone angles, mostly at values lower than  
 175  $40^\circ$ . Jets are rarely detected during intervals with high cone angles. The jet probabili-  
 176 ty during high cone angles ( $> 50^\circ$ ) decreases for low Mach numbers ( $< 5$ ). During these  
 177 conditions, the probability to detect jets is roughly six to seven times lower compared  
 178 to times of low cone angle ( $< 40^\circ$ ) and high Mach numbers ( $> 5$ ). This value is simi-  
 179 lar to the probability of detecting jets downstream of the quasi-parallel shock compared  
 180 to the quasi-perpendicular shock found by Archer and Horbury (2013). The right plot  
 181 of Fig.2 also shows that the jet probability at low mach numbers ( $< 5$ ) is significantly  
 182 decreasing even for intermediate cone angles ( $30\text{--}50^\circ$ ).

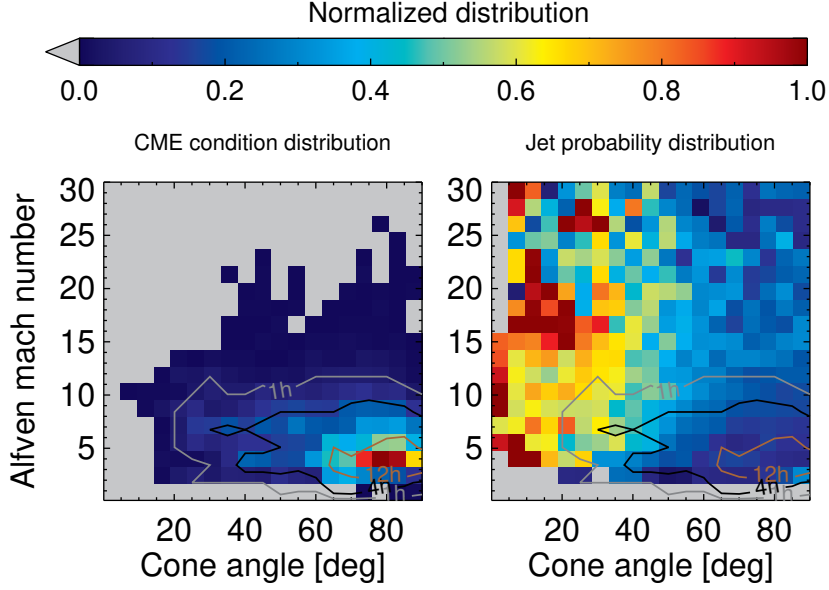


**Figure 3.** 2D histogram showing normalized distributions of cone angle and Mach number. The left plot shows the overall distribution of both parameter in the SW during CME-MEs. The right plot shows again the overall jet probability distribution (rightmost plot in Fig. 2), overlotted with contours of data availability during CME-MEs.

183 The mean SW conditions that we can find during CME-MEs is shown in the left  
 184 plot of Fig. 3. The same bin sizes from the previous plot ( $4.8^\circ$  for the x-axis and 1.6  
 185 for the y axis) were chosen. The distribution is confined mostly to the area at cone an-  
 186 gle higher than  $60^\circ$  and Mach numbers between 2 and 5.

187 The right plot of Fig. 3 is the same as the right plot of Fig. 2, showing the jet prob-  
 188 ability distribution, however, overlaid with the contours for the mean SW conditions found  
 189 during CME-MEs using the values taken from the left plot of Fig. 3. The innermost con-  
 190 tour (in brown) reveals CME-ME bins with data availabilities of more than 12 h. Again,  
 191 the distribution is confined mostly to the area at the lower right corner of the 2D-histogram  
 192 plot. The SW conditions during CMEs overlay the area where we find the lowest prob-  
 193 ability of detecting jets.

## 194 5 Discussion and Conclusion

195 For the first time, we analyze how the distinct conditions within CME-MEs influ-  
 196 ence the parameters necessary to produce jets efficiently. We suggest that the high IMF  
 197 cone angle found in the CME-MEs renders the building of a foreshock difficult. In ad-  
 198 dition to this, sufficiently weak Mach numbers might hinder the backstreaming of ions  
 199 and thus the building of the foreshock and the reformation of the quasi-parallel shock.

200 Our findings are further supported by simulation results done by Tinoco-Arenas  
 201 et al. (2022). The appearance of jets ceased at shocks with very low Alfvén Mach num-  
 202 bers. Similarly, high  $\Theta_{Bn}$  angles (here as a proxy we use the cone angle at the subsol-  
 203 ar point) caused a reduction of jet production in their simulations.

204 While the number of detected jets is significantly lower within CMEs (Koller et al.,  
 205 2022), there is still a non-vanishing amount of them. Whether these jets are different com-  
 206 pared to jets during low- cone angle and high-Alfvénic conditions will give insight in their  
 207 generation mechanisms. The overall probability distribution of jets that were only de-  
 208 tected during CME-MEs (not shown) follows the same probability distribution as shown  
 209 in the right plot of Fig. 2. The only significant difference being that the favorable con-  
 210 ditions for the jet generation are rarer within CME-MEs.

211 With  $\Theta_{Bn}$  (and as proxy the cone angle) having the most influence on the jet pro-  
 212 duction, there is the question whether the foreshock builds up at positions far away from  
 213 the Earth-Sun line (as sketched in Fig. 1 by Vuorinen et al., 2019).

214 At the planet Mercury, we also find low Alfvénic Mach numbers similar to what  
 215 we find within CME-MEs at 1 AU. Karlsson et al. (2016) analyzed isolated magnetic field  
 216 structures within the Hermean magnetosheath (Anderson et al., 2010) as possible ana-  
 217 logues to terrestrial jets. However, the analyzed structures had no dependence on the  
 218  $\Theta_{Bn}$  distribution, making the connection to the classical magnetosheath jets detected  
 219 at Earth uncertain. Sundberg et al. (2015) suggested that the low mach number might  
 220 not lead to a proper foreshock. This could be similar to what we see at the Earth’s bow  
 221 shock during CME-MEs. Based on our result, we postulate that the number of jets within  
 222 the Hermean magnetosheath would be low. The BepiColombo mission will insert into  
 223 an orbit around Mercury between December 2025 and March 2026 (Milillo et al., 2020).  
 224 This mission will give new insights on the jet occurrence and generation at the Hermean  
 225 magnetosheath and foreshock.

226 In summary, we show that a mix of high cone angles and low Mach numbers are  
 227 unfavorable SW conditions, hence, decreasing the production of jets in the magnetosheath.  
 228 The condition within CME-MEs is similar to this condition, which gives context to the  
 229 low detection number of jets in this structure as was reported by Koller et al. (2022). With-  
 230 out a proper foreshock, the proposed jet generation mechanisms for the majority of jets  
 231 is not applicable. Further investigation into the exact details is necessary to conclude,  
 232 how the CME is disrupting the foreshock. Future case studies as well as simulations on  
 233 the interaction of CMEs with the bow shock can complement our statistical work. A next  
 234 step is to analyze, whether the jets found during different structures have statistically  
 235 distinctive differences in their properties.

## 236 Data Availability Statement

237 We thank C. W. Carlson and J. P. McFadden for use of ESA data. We acknowl-  
 238 edge the use of NASA/ GSFC’s Space Physics Data Facility’s OMNI data and web ser-  
 239 vices ([https://omniweb.gsfc.nasa.gov/html/omni\\_min\\_data.html](https://omniweb.gsfc.nasa.gov/html/omni_min_data.html)). THEMIS and  
 240 OMNI data were accessed using the SPEDAS software (Angelopoulos et al., 2019). We  
 241 provide the jet lists as well as the magnetosheath times at <https://osf.io/hwkum/>.

## 242 Acknowledgments

243 F.K., M.T., L.P., O.R., and F.P. gratefully acknowledge the Austrian Science Fund (FWF):  
 244 P 33285-N for supporting this project. We acknowledge NASA contract NAS5-02099 and  
 245 V. Angelopoulos for use of data from the THEMIS Mission. Specifically we thank K.H.  
 246 Glassmeier, H.U. Auster and W. Baumjohann for the use of FGM data provided under  
 247 the lead of the Technical University of Braunschweig and with financial support through  
 248 the German Ministry for Economy and Technology and the German Center for Aviation  
 249 and Space (DLR) under contract 50 OC 0302.

250 **References**

- 251 Anderson, B. J., Acuña, M. H., Korth, H., Slavin, J. A., Uno, H., Johnson, C. L., ...  
 252 McNutt, R. L. (2010, May). The Magnetic Field of Mercury. *Space Science*  
 253 *Reviews*, 152(1-4), 307-339. doi: 10.1007/s11214-009-9544-3
- 254 Angelopoulos, V. (2008, December). The THEMIS Mission. *Space Science Reviews*,  
 255 141(1-4), 5-34. doi: 10.1007/s11214-008-9336-1
- 256 Archer, M. O., & Horbury, T. S. (2013, February). Magnetosheath dynamic pressure  
 257 enhancements: occurrence and typical properties. *Annales Geophysicae*, 31(2),  
 258 319-331. doi: 10.5194/angeo-31-319-2013
- 259 Archer, M. O., Horbury, T. S., & Eastwood, J. P. (2012, May). Magnetosheath  
 260 pressure pulses: Generation downstream of the bow shock from solar wind  
 261 discontinuities. *Journal of Geophysical Research (Space Physics)*, 117(A5),  
 262 A05228. doi: 10.1029/2011JA017468
- 263 Auster, H. U., Glassmeier, K. H., Magnes, W., Aydogar, O., Baumjohann, W.,  
 264 Constantinescu, D., ... Wiedemann, M. (2008, December). The THEMIS  
 265 Fluxgate Magnetometer. *Space Science Reviews*, 141(1-4), 235-264. doi:  
 266 10.1007/s11214-008-9365-9
- 267 Balogh, A., & Treumann, R. A. (2013). *Physics of Collisionless Shocks* (Vol. 12).  
 268 doi: 10.1007/978-1-4614-6099-2
- 269 Cane, H. V., & Richardson, I. G. (2003, April). Interplanetary coronal mass ejections  
 270 in the near-Earth solar wind during 1996-2002. *Journal of Geophysical*  
 271 *Research (Space Physics)*, 108(A4), 1156. doi: 10.1029/2002JA009817
- 272 Hietala, H., Laitinen, T. V., Andréová, K., Vainio, R., Vaivads, A., Palmroth, M.,  
 273 ... Rème, H. (2009, December). Supermagnetosonic Jets behind a Collision-  
 274 less Quasiparallel Shock. *Physical Review Letters*, 103(24), 245001. doi:  
 275 10.1103/PhysRevLett.103.245001
- 276 Hietala, H., Phan, T. D., Angelopoulos, V., Oieroset, M., Archer, M. O., Karlsson,  
 277 T., & Plaschke, F. (2018, February). In Situ Observations of a Magnetosheath  
 278 High-Speed Jet Triggering Magnetopause Reconnection. *Geophysics Research*  
 279 *Letters*, 45(4), 1732-1740. doi: 10.1002/2017GL076525
- 280 Hietala, H., & Plaschke, F. (2013, November). On the generation of magnetosheath  
 281 high-speed jets by bow shock ripples. *Journal of Geophysical Research (Space*  
 282 *Physics)*, 118(11), 7237-7245. doi: 10.1002/2013JA019172
- 283 Karlsson, T., Kullen, A., Liljeblad, E., Brenning, N., Nilsson, H., Gunell, H., &  
 284 Hamrin, M. (2015, September). On the origin of magnetosheath plasmoids and  
 285 their relation to magnetosheath jets. *Journal of Geophysical Research (Space*  
 286 *Physics)*, 120(9), 7390-7403. doi: 10.1002/2015JA021487
- 287 Karlsson, T., Liljeblad, E., Kullen, A., Raines, J. M., Slavin, J. A., & Sundberg,  
 288 T. (2016, September). Isolated magnetic field structures in Mercury's mag-  
 289 netosheath as possible analogues for terrestrial magnetosheath plasmoids and  
 290 jets. *Planetary and Space Science*, 129, 61-73. doi: 10.1016/j.pss.2016.06.002
- 291 King, J. H., & Papitashvili, N. E. (2005, February). Solar wind spatial scales in and  
 292 comparisons of hourly Wind and ACE plasma and magnetic field data. *Jour-*  
 293 *nal of Geophysical Research (Space Physics)*, 110(A2), A02104. doi: 10.1029/  
 294 2004JA010649
- 295 Koller, F., Plaschke, F., Temmer, M., Preisser, L., Roberts, O. W., Weiss, S., &  
 296 Vörös, Z. (2022, Jul). *Themis local magnetosheath jet data 2008-2021*. OSF.  
 297 Retrieved from [osf.io/hwkum](https://osf.io/hwkum)
- 298 Koller, F., Temmer, M., Preisser, L., Plaschke, F., Geyer, P., Jian, L. K., ... LaM-  
 299 oury, A. T. (2022). Magnetosheath jet occurrence rate in relation to cmes and  
 300 sirs. *Journal of Geophysical Research: Space Physics*, 127(4), e2021JA030124.  
 301 Retrieved from [https://agupubs.onlinelibrary.wiley.com/doi/abs/](https://agupubs.onlinelibrary.wiley.com/doi/abs/10.1029/2021JA030124)  
 302 [10.1029/2021JA030124](https://doi.org/10.1029/2021JA030124) (e2021JA030124 2021JA030124) doi: [https://doi.org/](https://doi.org/10.1029/2021JA030124)  
 303 [10.1029/2021JA030124](https://doi.org/10.1029/2021JA030124)
- 304 LaMoury, A. T., Hietala, H., Plaschke, F., Vuorinen, L., & Eastwood, J. P. (2021).

- 305 Solar wind control of magnetosheath jet formation and propagation to the  
 306 magnetopause. *Journal of Geophysical Research: Space Physics*, 126(9),  
 307 e2021JA029592. Retrieved from [https://agupubs.onlinelibrary.wiley](https://agupubs.onlinelibrary.wiley.com/doi/abs/10.1029/2021JA029592)  
 308 [.com/doi/abs/10.1029/2021JA029592](https://doi.org/10.1029/2021JA029592) (e2021JA029592 2021JA029592) doi:  
 309 <https://doi.org/10.1029/2021JA029592>
- 310 McFadden, J. P., Carlson, C. W., Larson, D., Ludlam, M., Abiad, R., Elliott, B., ...  
 311 Angelopoulos, V. (2008, December). The THEMIS ESA Plasma Instrument  
 312 and In-flight Calibration. *Space Science Reviews*, 141(1-4), 277-302. doi:  
 313 10.1007/s11214-008-9440-2
- 314 Milillo, A., Fujimoto, M., Murakami, G., Benkhoff, J., Zender, J., Aizawa, S., ...  
 315 Wahlund, J. E. (2020, July). Investigating Mercury's Environment with the  
 316 Two-Spacecraft BepiColombo Mission. *Space Science Reviews*, 216(5), 93. doi:  
 317 10.1007/s11214-020-00712-8
- 318 Norenius, L., Hamrin, M., Goncharov, O., Gunell, H., Opgenoorth, H., Pitkänen,  
 319 T., ... Baddeley, L. (2021, August). Ground-Based Magnetometer Response  
 320 to Impacting Magnetosheath Jets. *Journal of Geophysical Research (Space*  
 321 *Physics)*, 126(8), e29115. doi: 10.1029/2021JA029115
- 322 Němeček, Z., Šafránková, J., Přejch, L., Sibeck, D. G., Kokubun, S., & Mukai, T.  
 323 (1998, January). Transient flux enhancements in the magnetosheath. *Geo-*  
 324 *physics Research Letters*, 25(8), 1273-1276. doi: 10.1029/98GL50873
- 325 Nykyri, K., Bengtson, M., Angelopoulos, V., Nishimura, Y., & Wing, S. (2019,  
 326 June). Can Enhanced Flux Loading by High-Speed Jets Lead to a Substorm?  
 327 Multipoint Detection of the Christmas Day Substorm Onset at 08:17 UT,  
 328 2015. *Journal of Geophysical Research (Space Physics)*, 124(6), 4314-4340. doi:  
 329 10.1029/2018JA026357
- 330 Plaschke, F., Hietala, H., & Angelopoulos, V. (2013, October). Anti-sunward high-  
 331 speed jets in the subsolar magnetosheath. *Annales Geophysicae*, 31(10), 1877-  
 332 1889. doi: 10.5194/angeo-31-1877-2013
- 333 Plaschke, F., Hietala, H., Angelopoulos, V., & Nakamura, R. (2016, April). Geoeffec-  
 334 tive jets impacting the magnetopause are very common. *Journal of Geophysical*  
 335 *Research (Space Physics)*, 121(4), 3240-3253. doi: 10.1002/2016JA022534
- 336 Plaschke, F., Hietala, H., Archer, M., Blanco-Cano, X., Kajdič, P., Karlsson, T., ...  
 337 Sibeck, D. (2018, August). Jets Downstream of Collisionless Shocks. *Space*  
 338 *Science Reviews*, 214(5), 81. doi: 10.1007/s11214-018-0516-3
- 339 Plaschke, F., Hietala, H., & Vörös, Z. (2020, September). Scale Sizes of Mag-  
 340 netosheath Jets. *Journal of Geophysical Research (Space Physics)*, 125(9),  
 341 e27962. doi: 10.1029/2020JA027962
- 342 Preisser, L., Blanco-Cano, X., Kajdič, P., Burgess, D., & Trotta, D. (2020, Septem-  
 343 ber). Magnetosheath Jets and Plasmoids: Characteristics and Formation  
 344 Mechanisms from Hybrid Simulations. *The Astrophysical Journal Letters*,  
 345 900(1), L6. doi: 10.3847/2041-8213/abad2b
- 346 Raptis, S., Karlsson, T., Plaschke, F., Kullen, A., & Lindqvist, P.-A. (2020, Novem-  
 347 ber). Classifying Magnetosheath Jets Using MMS: Statistical Properties. *Jour-*  
 348 *nal of Geophysical Research (Space Physics)*, 125(11), e27754. doi: 10.1029/  
 349 2019JA027754
- 350 Raptis, S., Karlsson, T., Vaivads, A., Pollock, C., Plaschke, F., Johlander, A., ...  
 351 Lindqvist, P.-A. (2022, December). Downstream high-speed plasma jet gener-  
 352 ation as a direct consequence of shock reformation. *Nature Communications*,  
 353 13(1), 598. Retrieved 2022-03-13, from [https://www.nature.com/articles/](https://www.nature.com/articles/s41467-022-28110-4)  
 354 [s41467-022-28110-4](https://doi.org/10.1038/s41467-022-28110-4) doi: 10.1038/s41467-022-28110-4
- 355 Richardson, I. G., & Cane, H. V. (2010, June). Near-Earth Interplanetary Coronal  
 356 Mass Ejections During Solar Cycle 23 (1996 - 2009): Catalog and Summary of  
 357 Properties. *Solar Physics*, 264(1), 189-237. doi: 10.1007/s11207-010-9568-6
- 358 Schwartz, S. J., & Burgess, D. (1991, March). Quasi-parallel shocks: A patchwork  
 359 of three-dimensional structures. *Geophysical Research Letters*, 18(3), 373-376.

- 360 doi: 10.1029/91GL00138
- 361 Stone, E. C., Frandsen, A. M., Mewaldt, R. A., Christian, E. R., Margolies, D.,  
362 Ormes, J. F., & Snow, F. (1998, July). The Advanced Composition Explorer.  
363 *Space Science Reviews*, 86, 1-22. doi: 10.1023/A:1005082526237
- 364 Sundberg, T., Boardsen, S. A., Burgess, D., & Slavin, J. A. (2015, September). Co-  
365 herent wave activity in Mercury's magnetosheath. *Journal of Geophysical Re-*  
366 *search (Space Physics)*, 120(9), 7342-7356. doi: 10.1002/2015JA021499
- 367 Suni, J., Palmroth, M., Turc, L., Battarbee, M., Johlander, A., Tarvus, V., ...  
368 Zhou, H. (2021, October). Connection Between Foreshock Structures and the  
369 Generation of Magnetosheath Jets: Vlasiator Results. *Geophysical Research*  
370 *Letters*, 48(20), e95655. doi: 10.1029/2021GL095655
- 371 Temmer, M., & Bothmer, V. (2022, February). Characteristics and evolution of  
372 sheath and leading edge structures of interplanetary coronal mass ejections in  
373 the inner heliosphere based on Helios and Parker Solar Probe observations.  
374 *arXiv e-prints*, arXiv:2202.04391.
- 375 Tinoco-Arenas, A., Kajdič, P., Preisser, L., Blanco-Cano, X., Trotta, D., & Burgess,  
376 D. (2022, February). Parametric study of magnetosheath jets in 2D local  
377 hybrid simulations. *Frontiers in Astronomy and Space Sciences*, 9, 5. doi:  
378 10.3389/fspas.2022.793195
- 379 Vuorinen, L., Hietala, H., & Plaschke, F. (2019, August). Jets in the magnetosheath:  
380 IMF control of where they occur. *Annales Geophysicae*, 37(4), 689-697. doi: 10  
381 .5194/angeo-37-689-2019